Measurements of $e^+e^- \to K^0_S K^\pm \pi^\mp \pi^0$ and $K^0_S K^\pm \pi^\mp \eta$ at center-of-mass energies from 3.90 to 4.60 GeV

M. Ablikim,[1] M. N. Achasov,[10,d] S. Ahmed,[15] M. Albrecht,[4] M. Alekseev,[55a,55c] A. Amoroso,[55a,55c] F. F. An,[1] Q. An,[52,42] Y. Bai,[41] O. Bakina,[27] R. Baldini Ferroli,[23a] Y. Ban,[35] K. Begzsuren,[25] D. W. Bennett,[22] J. V. Bennett,[5] N. Berger,[26] M. Bertani,[23a] D. Bettoni,[24a] F. Bianchi,[55a,55c] I. Boyko,[27] R. A. Briere,[5] H. Cai,[57] X. Cai,[1,42] A. Calcaterra,[23a] G. F. Cao,[1,46] S. A. Cetin,[45b] J. Chai,[55c] J. F. Chang,[1,42] W. L. Chang,[1,46] G. Chelkov,[27,b,c] G. Chen,[1] H. S. Chen,[1,46] J. C. Chen,[1] M. L. Chen,[1,42] P. L. Chen,[53] S. J. Chen,[33] Y. B. Chen,[1,42] W. Cheng,[55c] G. Cibinetto,[24a] F. Cossio,[55c] H. L. Dai,[1,42] J. P. Dai,[37,h] A. Dbeyssi,[15] D. Dedovich,[27] Z. Y. Deng,[1] A. Denig,[26] I. Denysenko,[27] M. Destefanis,[55a,55c] F. De Mori,[55a,55c] Y. Ding,[31] C. Dong,[34] J. Dong,[1,42] L. Y. Dong,[1,46] M. Y. Dong,[1,42,46] Z. L. Dou,[33] S. X. Du,[60] P. F. Duan,[1] J. Z. Fan,[44] J. Fang,[1,42] S. S. Fang,[1,46] Y. Fang,[1] R. Farinelli,[24a,24b] L. Fava,[55b,55c] S. Fegan,[26] F. Feldbauer,[4] G. Felici,[23a] C. Q. Feng,[52,42] M. Fritsch,[4] C. D. Fu,[1] Y. Fu,[1] Q. Gao,[1] X. L. Gao,[52,42] Y. Gao,[44] Y. G. Gao,[6] Z. Gao,[52,42] B. Garillon,[26] I. Garzia,[24a] A. Gilman,[49] K. Goetzen,[11] L. Gong,[34] W. X. Gong,[1,42] W. Gradl,[26] M. Greco,[55a,55c] L. M. Gu,[33] M. H. Gu,[1,42] Y. T. Gu,[13] A. Q. Guo,[1] L. B. Guo,[32] R. P. Guo,[1,46] Y. P. Guo,[26] A. Guskov,[27] Z. Haddadi,[29] S. Han,[57] X. Q. Hao,[16] F. A. Harris,[47] K. L. He,[1,46] F. H. Heinsius,[4] T. Held,[4] Y. K. Heng,[1,42,46] Z. L. Hou,[1] H. M. Hu,[1,46] J. F. Hu,[37,h] T. Hu,[1,42,46] Y. Hu,[1] G. S. Huang,[52,42] J. S. Huang,[16] X. T. Huang,[36] X. Z. Huang,[33] Z. L. Huang,[31] T. Hussain,[54] N. Hsken,[50] W. Ikegami Andersson,[56] M. Irshad,[52,42] Q. Ji,[1] Q. P. Ji,[16] X. B. Ji,[1,46] X. L. Ji,[1,42] X. S. Jiang,[1,42,46] X. Y. Jiang,[34] J. B. Jiao,[36] Z. Jiao,[18] D. P. Jin,[1,42,46] S. Jin,[33] Y. Jin,[48] T. Johansson,[56] A. Julin,[49] N. Kalantar-Nayestanaki,[29] X. S. Kang,[34] M. Kavatsyuk,[29] B. C. Ke,[1] I. K. Keshk,[4] T. Khan,[52,42] A. Khoukaz,[50] P. Kiese,[26] R. Kiuchi,[1] R. Kliemt,[11] L. Koch,[28] O. B. Kolcu,[45b,f] B. Kopf,[4] M. Kornicer,[47] M. Kuemmel,[4] M. Kuessner,[4] A. Kupsc,[56] M. Kurth,[1] W. Kühn,[28] J. S. Lange,[28] P. Larin,[15] L. Lavezzi,[55c] S. Leiber,[4] H. Leithoff,[26] C. Li,[56] Cheng Li,[52,42] D. M. Li,[60] F. Li,[1,42] F. Y. Li,[35] G. Li,[1] H. B. Li,[1,46] H. J. Li,[1,46] J. C. Li,[1] J. W. Li,[40] Ke Li,[1] Lei Li,[3] P. L. Li,[52,42] P. R. Li,[46,7] Q. Y. Li,[36] T. Li,[36] W. D. Li,[1,46] W. G. Li,[1] X. L. Li,[36] X. N. Li,[1,42] X. Q. Li,[34] Z. B. Li,[43] H. Liang,[52,42] Y. F. Liang,[39] Y. T. Liang,[28] G. R. Liao,[12] L. Z. Liao,[1,46] J. Libby,[21] C. X. Lin,[43] D. X. Lin,[15] B. Liu,[37,h] B. J. Liu,[1] C. X. Liu,[1] D. Liu,[52,42] D. Y. Liu,[37,h] F. H. Liu,[38] Fang Liu,[1] Feng Liu,[6] H. B. Liu,[13] H. L. Liu,[41] H. M. Liu,[1,46] Huanhuan Liu,[1] Huihui Liu,[17] J. B. Liu,[52,42] J. Y. Liu,[1,46] K. Y. Liu,[31] Ke Liu,[6] Q. Liu,[46] S. B. Liu,[52,42] X. Liu,[30] Y. B. Liu,[34] Z. A. Liu,[1,42,46] Zhiqing Liu,[26] Y. F. Long,[35] X. C. Lou,[1,42,46] H. J. Lu,[18] J. D. Lu,[1,46] J. G. Lu,[1,42] Y. Lu,[1] Y. P. Lu,[1,42] C. L. Luo,[32] M. X. Luo,[59] T. Luo,[9,j] X. L. Luo,[1,42] S. Lusso,[55c] X. R. Lyu,[46] F. C. Ma,[31] H. L. Ma,[1] L. L. Ma,[36] M. M. Ma,[1,46] Q. M. Ma,[1] X. N. Ma,[34] X. X. Ma,[1,46] X. Y. Ma,[1,42] Y. M. Ma,[36] F. E. Maas,[15] M. Maggiora,[55a,55c] S. Maldaner,[26] Q. A. Malik,[54] A. Mangoni,[23b] Y. J. Mao,[35] Z. P. Mao,[1] S. Marcello,[55a,55c] Z. X. Meng,[48] J. G. Messchendorp,[29] G. Mezzadri,[24a] J. Min,[1,42] T. J. Min,[33] R. E. Mitchell,[22] X. H. Mo,[1,42,46] Y. J. Mo,[6] C. Morales Morales,[15] N. Yu. Muchnoi,[10,d] H. Muramatsu,[49] A. Mustafa,[4] S. Nakhoul,[11,g] Y. Nefedov,[27] F. Nerling,[11,g] I. B. Nikolaev,[10,d] Z. Ning,[1,42] S. Nisar,[8,k] S. L. Niu,[1,42] S. L. Olsen,[46] Q. Ouyang,[1,42,46] S. Pacetti,[23b] Y. Pan,[52,42] M. Papenbrock,[56] P. Patteri,[23a] M. Pelizaeus,[4] J. Pellegrino,[55a,55c] H. P. Peng,[52,42] K. Peters,[11,g] J. Pettersson,[56] J. L. Ping,[32] R. G. Ping,[1,46] A. Pitka,[4] R. Poling,[49] V. Prasad,[52,42] H. R. Qi,[2] M. Qi,[33] T. Y. Qi,[2] S. Qian,[1,42] C. F. Qiao,[46] N. Qin,[57] X. S. Qin,[4] Z. H. Qin,[1,42] J. F. Qiu,[1] S. Q. Qu,[34] K. H. Rashid,[54,i] C. F. Redmer,[26] M. Richter,[4] M. Ripka,[26] A. Rivetti,[55c] M. Rolo,[55c] G. Rong,[1,46] Ch. Rosner,[15] M. Rump,[50] A. Sarantsev,[27,e] M. Savrié,[24b] K. Schoenning,[56] W. Shan,[19] X. Y. Shan,[52,42] M. Shao,[52,42] C. P. Shen,[2] P. X. Shen,[34] X. Y. Shen,[1,46] H. Y. Sheng,[1] X. Shi,[1,42] J. J. Song,[36] W. M. Song,[36] X. Y. Song,[1] S. Sosio,[55a,55c] C. Sowa,[4] S. Spataro,[55a,55c] G. X. Sun,[1] J. F. Sun,[16] L. Sun,[57] S. S. Sun,[1,46] X. H. Sun,[1] Y. J. Sun,[52,42] Y. K. Sun,[52,42] Y. Z. Sun,[1] Z. J. Sun,[1,42] Z. T. Sun,[1] Y. T. Tan,[52,42] C. J. Tang,[39] G. Y. Tang,[1] X. Tang,[1] M. Tiemens,[29] B. Tsednee,[25] I. Uman,[45d] B. Wang,[1] B. L. Wang,[46] C. W. Wang,[33] D. Y. Wang,[35] Dan Wang,[46] K. Wang,[1,42] L. L. Wang,[1] L. S. Wang,[1] M. Wang,[36] Meng Wang,[1,46] P. Wang,[1] P. L. Wang,[1] W. P. Wang,[52,42] X. F. Wang,[1] Y. Wang,[52,42] Y. F. Wang,[1,42,46] Z. Wang,[1,42] Z. G. Wang,[1,42] Z. Y. Wang,[1] Zongyuan Wang,[1,46] T. Weber,[4] D. H. Wei,[12] P. Weidenkaff,[26] S. P. Wen,[1] U. Wiedner,[4] M. Wolke,[56] L. H. Wu,[1] L. J. Wu,[1,46] Z. Wu,[1,42] L. Xia,[52,42] X. Xia,[36] Y. Xia,[20] D. Xiao,[1] Y. J. Xiao,[1,46] Z. J. Xiao,[32] Y. G. Xie,[1,42] Y. H. Xie,[6] X. A. Xiong,[1,46] Q. L. Xiu,[1,42] G. F. Xu,[1] J. J. Xu,[1,46] L. Xu,[1] Q. J. Xu,[14] X. P. Xu,[40] F. Yan,[53] L. Yan,[55a,55c] W. B. Yan,[52,42] W. C. Yan,[2] Y. H. Yan,[20] H. J. Yang,[37,h] H. X. Yang,[1] L. Yang,[57] R. X. Yang,[52,42] S. L. Yang,[1,46] Y. H. Yang,[33] Y. X. Yang,[12] Yifan Yang,[1,46] Z. Q. Yang,[20] M. Ye,[1,42] M. H. Ye,[7] J. H. Yin,[1] Z. Y. You,[43] B. X. Yu,[1,42,46] C. X. Yu,[34] J. S. Yu,[20] C. Z. Yuan,[1,46] Y. Yuan,[1] A. Yuncu,[45b,a] A. A. Zafar,[54] Y. Zeng,[20] B. X. Zhang,[1] B. Y. Zhang,[1,42] C. C. Zhang,[1] D. H. Zhang,[1] H. H. Zhang,[43] H. Y. Zhang,[1,42] J. Zhang,[1,46] J. L. Zhang,[58] J. Q. Zhang,[4] J. W. Zhang,[1,42,46] J. Y. Zhang,[1] J. Z. Zhang,[1,46] K. Zhang,[1,46] L. Zhang,[44] S. F. Zhang,[33] T. J. Zhang,[37,h] X. Y. Zhang,[36] Y. Zhang,[52,42] Y. H. Zhang,[1,42] Y. T. Zhang,[52,42] Yang Zhang,[1] Yao Zhang,[1] Yu Zhang,[46] Z. H. Zhang,[6] Z. P. Zhang,[52] Z. Y. Zhang,[57] G. Zhao,[1] J. W. Zhao,[1,42] J. Y. Zhao,[1,46] J. Z. Zhao,[1,42] Lei Zhao,[52,42] Ling Zhao,[1] M. G. Zhao,[34] Q. Zhao,[1] S. J. Zhao,[60] T. C. Zhao,[1] Y. B. Zhao,[1,42] Z. G. Zhao,[52,42] A. Zhemchugov,[27,b] B. Zheng,[53] J. P. Zheng,[1,42] W. J. Zheng,[36] Y. H. Zheng,[46] B. Zhong,[32] L. Zhou,[1,42] Q. Zhou,[1,46] X. Zhou,[57] X. K. Zhou,[52,42] X. R. Zhou,[52,42]

X. Y. Zhou,[1] Xiaoyu Zhou,[20] Xu Zhou,[20] A. N. Zhu,[1,46] J. Zhu,[34] J. Zhu,[43] K. Zhu,[1] K. J. Zhu,[1,42,46] S. Zhu,[1] S. H. Zhu,[51] X. L. Zhu,[44] Y. C. Zhu,[52,42] Y. S. Zhu,[1,46] Z. A. Zhu,[1,46] J. Zhuang,[1,42] B. S. Zou,[1] and J. H. Zou[1]

(BESIII Collaboration)

[1]*Institute of High Energy Physics, Beijing 100049, People's Republic of China*
[2]*Beihang University, Beijing 100191, People's Republic of China*
[3]*Beijing Institute of Petrochemical Technology, Beijing 102617, People's Republic of China*
[4]*Bochum Ruhr-University, D-44780 Bochum, Germany*
[5]*Carnegie Mellon University, Pittsburgh, Pennsylvania 15213, USA*
[6]*Central China Normal University, Wuhan 430079, People's Republic of China*
[7]*China Center of Advanced Science and Technology, Beijing 100190, People's Republic of China*
[8]*COMSATS University Islamabad, Lahore Campus, Defence Road, Off Raiwind Road, 54000 Lahore, Pakistan*
[9]*Fudan University, Shanghai 200443, People's Republic of China*
[10]*G.I. Budker Institute of Nuclear Physics SB RAS (BINP), Novosibirsk 630090, Russia*
[11]*GSI Helmholtzcentre for Heavy Ion Research GmbH, D-64291 Darmstadt, Germany*
[12]*Guangxi Normal University, Guilin 541004, People's Republic of China*
[13]*Guangxi University, Nanning 530004, People's Republic of China*
[14]*Hangzhou Normal University, Hangzhou 310036, People's Republic of China*
[15]*Helmholtz Institute Mainz, Johann-Joachim-Becher-Weg 45, D-55099 Mainz, Germany*
[16]*Henan Normal University, Xinxiang 453007, People's Republic of China*
[17]*Henan University of Science and Technology, Luoyang 471003, People's Republic of China*
[18]*Huangshan College, Huangshan 245000, People's Republic of China*
[19]*Hunan Normal University, Changsha 410081, People's Republic of China*
[20]*Hunan University, Changsha 410082, People's Republic of China*
[21]*Indian Institute of Technology Madras, Chennai 600036, India*
[22]*Indiana University, Bloomington, Indiana 47405, USA*
[23a]*INFN Laboratori Nazionali di Frascati, I-00044, Frascati, Italy*
[23b]*INFN and University of Perugia, I-06100, Perugia, Italy*
[24a]*INFN Sezione di Ferrara, I-44122, Ferrara, Italy*
[24b]*University of Ferrara, I-44122, Ferrara, Italy*
[25]*Institute of Physics and Technology, Peace Ave. 54B, Ulaanbaatar 13330, Mongolia*
[26]*Johannes Gutenberg University of Mainz, Johann-Joachim-Becher-Weg 45, D-55099 Mainz, Germany*
[27]*Joint Institute for Nuclear Research, 141980 Dubna, Moscow region, Russia*
[28]*Justus-Liebig-Universitaet Giessen, II. Physikalisches Institut, Heinrich-Buff-Ring 16, D-35392 Giessen, Germany*
[29]*KVI-CART, University of Groningen, NL-9747 AA Groningen, The Netherlands*
[30]*Lanzhou University, Lanzhou 730000, People's Republic of China*
[31]*Liaoning University, Shenyang 110036, People's Republic of China*
[32]*Nanjing Normal University, Nanjing 210023, People's Republic of China*
[33]*Nanjing University, Nanjing 210093, People's Republic of China*
[34]*Nankai University, Tianjin 300071, People's Republic of China*
[35]*Peking University, Beijing 100871, People's Republic of China*
[36]*Shandong University, Jinan 250100, People's Republic of China*
[37]*Shanghai Jiao Tong University, Shanghai 200240, People's Republic of China*
[38]*Shanxi University, Taiyuan 030006, People's Republic of China*
[39]*Sichuan University, Chengdu 610064, People's Republic of China*
[40]*Soochow University, Suzhou 215006, People's Republic of China*
[41]*Southeast University, Nanjing 211100, People's Republic of China*
[42]*State Key Laboratory of Particle Detection and Electronics, Beijing 100049, Hefei 230026, People's Republic of China*
[43]*Sun Yat-Sen University, Guangzhou 510275, People's Republic of China*
[44]*Tsinghua University, Beijing 100084, People's Republic of China*
[45a]*Ankara University, 06100 Tandogan, Ankara, Turkey*
[45b]*Istanbul Bilgi University, 34060 Eyup, Istanbul, Turkey*
[45c]*Uludag University, 16059 Bursa, Turkey*
[45d]*Near East University, Nicosia, North Cyprus, Mersin 10, Turkey*
[46]*University of Chinese Academy of Sciences, Beijing 100049, People's Republic of China*
[47]*University of Hawaii, Honolulu, Hawaii 96822, USA*

[48]University of Jinan, Jinan 250022, People's Republic of China
[49]University of Minnesota, Minneapolis, Minnesota 55455, USA
[50]University of Muenster, Wilhelm-Klemm-Str. 9, 48149 Muenster, Germany
[51]University of Science and Technology Liaoning, Anshan 114051, People's Republic of China
[52]University of Science and Technology of China, Hefei 230026, People's Republic of China
[53]University of South China, Hengyang 421001, People's Republic of China
[54]University of the Punjab, Lahore-54590, Pakistan
[55a]University of Turin, I-10125, Turin, Italy
[55b]University of Eastern Piedmont, I-15121, Alessandria, Italy
[55c]INFN, I-10125, Turin, Italy
[56]Uppsala University, Box 516, SE-75120 Uppsala, Sweden
[57]Wuhan University, Wuhan 430072, People's Republic of China
[58]Xinyang Normal University, Xinyang 464000, People's Republic of China
[59]Zhejiang University, Hangzhou 310027, People's Republic of China
[60]Zhengzhou University, Zhengzhou 450001, People's Republic of China

(Received 23 October 2018; published 9 January 2019)

Using 5.2 fb^{-1} e^+e^- annihilation data samples collected with the BESIII detector, we measure the cross sections of $e^+e^- \to K^0_S K^\pm \pi^\mp \pi^0$ and $K^0_S K^\pm \pi^\mp \eta$ at center-of-mass energies from 3.90 to 4.60 GeV. In addition, we search for the charmoniumlike resonance $Y(4260)$ decays into $K^0_S K^\pm \pi^\mp \pi^0$ and $K^0_S K^\pm \pi^\mp \eta$, and $Z_c^{0,\pm}(3900)$ decays into $K^0_S K^\pm \pi^{\mp,0}$ and $K^0_S K^\pm \eta$. Corresponding upper limits are provided since no clear signal is observed.

DOI: 10.1103/PhysRevD.99.012003

I. INTRODUCTION

With the experimental progress in the past decade, many charmoniumlike (XYZ) states were observed, which can not be accommodated within the naive quark model and are proposed as the candidate of the hidden-charm exotic mesons [1,2]. In this paper, we focus on the exotic states $Y(4260)$ and $Z_c(3900)$.

$Y(4260)$ was first observed in initial state radiation (ISR) process $e^+e^- \to \gamma_{\rm ISR}\pi^+\pi^- J/\psi$ by *BABAR* [3] and confirmed by CLEO [4], Belle [5] and another study of *BABAR* [6] in its decay into $\pi^+\ \pi^-\ J/\psi$. In later experiments, $Y(4260)$ was also observed in $Y(4260) \to \pi^0\pi^0 J/\psi$ [7]. Besides, some similar states are observed in final states, such as $\omega\chi_{c0}$ [8], $\pi^+\pi^- J/\psi$ [9], $\pi^+\pi^-\psi(3686)$ [10], $\pi^+\pi^- h_c$ [11], $\pi^+ D^0 D^{*-}$ [12] around 4.23 GeV. No further open-charm [13–19], hidden-charm [20,21] and charmless [22–24] decay modes have be seen. Different interpretations were proposed to explain its structure, such as the charmonium states $4\ ^3S_1$ [25–27] and $3\ ^3D_1$ [28], hybrid charmonium [29,30], tetraquark state [31–34], molecular state [35–40], and nonresonance explanation [41–43].

The $Z_c(3900)$ was observed in the $J/\psi\pi^\pm$ invariant mass distribution of the $e^+e^- \to \pi^+\pi^- J/\psi$ process by the BESIII Collaboration [44]. Subsequently, additional $Z_c(3900)$ decay channels were observed in $D\bar{D}^* + c.c.$ [45–47]. The J^P of $Z_c(3900)$ was determined to be 1^+ with a partial wave analysis of the $\pi^+\pi^- J/\psi$ final state [48]. Since its discovery, many interpretations on the nature of the $Z_c(3900)$ have been proposed, such as a $D\bar{D}^*$ molecule [49], a tetraquark state [50], a cusp effect [51], and dynamical generation through threshold effects [52,53].

[a]Also at Bogazici University, 34342 Istanbul, Turkey.
[b]Also at the Moscow Institute of Physics and Technology, Moscow 141700, Russia.
[c]Also at the Functional Electronics Laboratory, Tomsk State University, Tomsk, 634050, Russia.
[d]Also at the Novosibirsk State University, Novosibirsk, 630090, Russia.
[e]Also at the NRC "Kurchatov Institute", PNPI, 188300, Gatchina, Russia.
[f]Also at Istanbul Arel University, 34295 Istanbul, Turkey.
[g]Also at Goethe University Frankfurt, 60323 Frankfurt am Main, Germany.
[h]Also at Key Laboratory for Particle Physics, Astrophysics and Cosmology, Ministry. of Education; Shanghai Key Laboratory for Particle Physics and Cosmology; Institute of Nuclear and Particle Physics, Shanghai 200240, People's Republic of China.
[i]Also at Government College Women University, Sialkot - 51310, Punjab, Pakistan.
[j]Also at Key Laboratory of Nuclear Physics and Ion-beam Application (MOE) and Institute of Modern Physics, Fudan University, Shanghai 200443, People's Republic of China.
[k]Also at Harvard University, Department of Physics, Cambridge, Massachusetts 02138, USA.

Despite many interpretations, the natures of the $Y(4260)$ and $Z_c(3900)$ are still unclear. To comprehend these states, it is necessary to study more decay modes. All of the observed decay modes of the $Y(4260)$ and $Z_c(3900)$ are associated with the charm sector and no light hadron decay modes have been found yet [54–56]. A search for light hadron decay modes of the $Y(4260)$ and $Z_c(3900)$ is complementary to previous studies and may help to distinguish between different theoretical models and to understand strong interaction effects in this energy region. Among the large number of potential light hadron decay modes, the branching fractions (BFs) of charmonium states decaying into $K_S K^{\pm}\pi^{\mp}\pi^0$ and $K_S K^{\pm}\pi^{\mp}\eta$ are usually large [57]. In four-body final state, there should be abundant intermediate states, which may supply more possible decay channels for searching $Y(4260)$ and $Z_c(3900)$. Furthermore, the existence of charged and neutral pions in the final states enables a study of isospin multiplets. In this paper, we present a measurement of the Born cross sections ($\sigma_{\rm B}$) for $e^+e^- \to K^0_S K^{\pm}\pi^{\mp}\pi^0$ and $K^0_S K^{\pm}\pi^{\mp}\eta$. We also report upper limits of $e^+e^- \to Y(4260) \to K^0_S K^{\pm}\pi^{\mp}\pi^0$, $e^+e^- \to Y(4260) \to K^0_S K^{\pm}\pi^{\mp}\eta$, $e^+e^- \to \pi^{\mp,0} Z_c(3900)^{\pm,0} \to K^0_S K^{\pm}\pi^{\mp}\pi^0$, and $e^+e^- \to \pi^{\mp} Z_c(3900)^{\pm} \to K^0_S K^{\pm}\pi^{\mp}\eta$.

II. DETECTORS AND DATA SAMPLES

The BESIII detector [58], operating at the BEPCII collider [59], is a general purpose spectrometer with a geometrical acceptance of 93% of 4π solid angle. It has four main components: (1) a small-cell, helium-based (60% He, 40% C_3H_8) multilayer drift chamber with 43 layers providing an average single-hit resolution of 135 μm, a momentum resolution of 0.5% at 1.0 GeV/c in a 1.0 T magnetic field, and a specific ionization energy loss (dE/dx) resolution better than 6%, (2) a time-of-flight (TOF) detector constructed of 5 cm thick plastic scintillators, with 176 strips of 2.4 m length in two layers in the barrel and 96 fans of the end caps with time resolutions of 80 and 110 ps, respectively, which provide a 2σ K/π separation for momenta up to $\sim$1.0 GeV/c, (3) an electromagnetic calorimeter (EMC) consisting of 6240 CsI crystals in a cylindrical barrel structure and two end caps with an energy resolution of 2.5% (5%) at 1.0 GeV and a position resolution of 6 mm (9 mm) in the barrel (end caps), and (4) a muon counter consisting of resistive plate chambers in nine barrel and eight end-cap layers, which provide a 2 cm position resolution. More details of the BESIII detector can be found in Ref. [58].

This analysis is based on 5.2 fb^{-1} e^+e^- annihilation data samples [60] collected with the BESIII detector at center-of-mass energies ($\sqrt{s}$) from 3.90 to 4.60 GeV [61], which are listed in Table I. Monte Carlo (MC) simulations are used to optimize the event selection criteria, to study the detector acceptance and to understand the potential backgrounds. The GEANT4-based [62] simulation software BOOST [63] is implemented to simulate the detector response, describe geometry and material, realize digitization, and incorporate time-dependent beam backgrounds. Six generic MC samples, equivalent to the integrated luminosity of the data at the energy points 4.009, 4.230, 4.260, 4.360, 4.420 and 4.600 GeV are generated to study the backgrounds. The primary known decay channels are

TABLE I. Data sets and results of the Born cross section measurement for $e^+e^- \to K^0_S K^{\pm}\pi^{\mp}\pi^0$. The table includes the integrated luminosity $\mathcal{L}$, the number of observed signals events $N_{\rm sig}$, the total efficiency ϵ, the ISR correction factor $(1+\delta^{\rm ISR})$, the vacuum polarization correction factor $\frac{1}{|1-\Pi(s)|^2}$, and the Born cross section $\sigma_{\rm B}$. The first errors are statistical and the second ones are systematic. The details of systematic uncertainties are described in Sec. III D.

$\sqrt{s}$ (GeV)	$\mathcal{L}$ (pb^{-1})	$N_{\rm sig}$	ϵ (%)	$(1+\delta^{\rm ISR})$	$\frac{1}{\lvert 1-\Pi(s)\rvert^2}$	$\sigma_{\rm B}$ (pb)
3.896	52.61	469 ± 22	16.76	1.03	1.05	$74.41 \pm 3.47 \pm 3.35$
4.008	481.96	3335 ± 58	16.41	1.05	1.04	$58.02 \pm 1.01 \pm 2.61$
4.086	52.63	307 ± 18	16.70	1.06	1.05	$47.52 \pm 2.73 \pm 2.14$
4.189	43.09	240 ± 16	16.31	1.08	1.06	$45.38 \pm 2.94 \pm 2.04$
4.208	54.55	269 ± 17	15.49	1.11	1.06	$40.95 \pm 2.50 \pm 1.84$
4.217	54.13	257 ± 16	16.03	1.11	1.06	$38.28 \pm 2.40 \pm 1.72$
4.226	1091.74	5235 ± 73	15.90	1.10	1.06	$39.23 \pm 0.55 \pm 1.77$
4.242	55.59	255 ± 16	16.02	1.10	1.06	$37.46 \pm 2.35 \pm 1.69$
4.258	825.67	3850 ± 63	15.52	1.12	1.05	$38.65 \pm 0.63 \pm 1.74$
4.308	44.90	199 ± 15	15.55	1.11	1.05	$36.86 \pm 2.62 \pm 1.66$
4.358	539.84	2167 ± 47	15.38	1.12	1.05	$33.53 \pm 0.72 \pm 1.51$
4.387	55.18	237 ± 16	16.00	1.15	1.05	$33.68 \pm 2.20 \pm 1.52$
4.416	1073.56	3934 ± 63	15.21	1.14	1.05	$30.38 \pm 0.49 \pm 1.37$
4.467	109.94	378 ± 20	15.87	1.17	1.06	$26.70 \pm 1.38 \pm 1.20$
4.527	109.98	364 ± 20	15.35	1.17	1.06	$26.51 \pm 1.40 \pm 1.19$
4.575	46.67	149 ± 13	15.15	1.19	1.06	$24.87 \pm 2.06 \pm 1.12$
4.600	566.93	1612 ± 41	15.49	1.16	1.06	$22.71 \pm 0.57 \pm 1.02$

generated using EVTGEN [64] with the BFs set to the world average values [57] while the unknown decay modes are generated with LUNDCHARM [65]. Continuum hadronic events are generated with KKMC [66] and QED processes such as Bhabha scattering, dimuon, and digamma events are generated with KKMC and BABAYAGA [67]. To study the efficiency of each final state, a sample of 1×10^5 signal events is generated at each energy point using KKMC, which simulates e^+e^- annihilation, including beam energy spread and ISR effects.

III. DATA ANALYSIS

A. Measurement of $\sigma_{\rm B}(e^+e^- \to K^0_S K^\pm \pi^\mp \pi^0)$ and $\sigma_{\rm B}(e^+e^- \to K^0_S K^\pm \pi^\mp \eta)$

Candidate events for $e^+e^- \to K^0_S K^\pm \pi^\mp \pi^0/\eta$, with $K^0_S \to \pi^+\pi^-$ and $\pi^0/\eta \to \gamma\gamma$ are selected according to the following steps. First, K^0_S candidates are selected by looping over all pairs of oppositely charged tracks, which are assumed to be pions. Next, primary and secondary vertex fits [68] are performed and the decay length of the secondary vertex fit is required to be greater than twice its uncertainty. Furthermore, the invariant mass of the pion pair is required to satisfy $|M(\pi^+\pi^-) - M_{K^0_S}| < 12$ MeV/c^2, where $M_{K^0_S}$ denotes the nominal mass of the K^0_S [57]. If there are multiple K^0_S candidates in one event, the one with the smallest χ^2 from the secondary vertex fit is selected.

In addition to the two charged tracks that make up the K^0_S, two oppositely charged tracks are required. For the latter two charged tracks, the polar angle θ must satisfy $|\cos\theta| < 0.93$ and the distance of closest approach to the interaction point must be less than 10.0 and 1.0 cm along the beam direction and in the plane perpendicular to the beam direction, respectively. The particle type for each charged track is determined by selecting the hypotheses with the highest probability, which is calculated with the combined information from TOF and dE/dx measurements for different particle hypotheses. One charged track must be identified as a kaon and the other as a pion.

Photons are reconstructed from clusters deposited in the EMC, with the energy measured in the TOF included to improve reconstruction efficiency and energy resolution. At least two photons are required per event. The energy of a photon candidate is required to be larger than 25 MeV in the barrel region ($|\cos\theta| < 0.80$) or 50 MeV in the end-cap region ($0.86 < |\cos\theta| < 0.92$). The cluster timing is required to be between 0 and 700 ns to suppress electronic noise and energy depositions unrelated to the event of interest. To eliminate showers associated with charged particles, the opening angle between a photon candidate and the extrapolated position of the closest charged track should be larger than 20 degrees.

Finally, a four-constraint (4C) kinematic fit imposing energy-momentum conservation is performed to the final states. Only events with $\chi^2_{\rm 4C} < 60$ are accepted. For events with more than two photon candidates, the photon pair with the smallest $\chi^2_{\rm 4C}$ from the kinematic fit is accepted. After the 4C kinematic fit, no peaking background is observed in the generic MC samples. The invariant mass distributions of $\pi^+\pi^-$ versus $\gamma\gamma$ and the projections onto $M(\pi^+\pi^-)$ and $M(\gamma\gamma)$ after 4C fit are shown in Fig. 1 (at 4.258 GeV as an example), in which obvious K^0_S and π^0/η peaks are observed. The signal regions are defined as $M(\pi^+\pi^-) \in (0.488, 0.508)$ GeV/c^2, $M(\gamma\gamma) \in (0.12, 0.15)$ GeV/c^2 (for the π^0 mode) and $M(\gamma\gamma) \in (0.52, 0.58)$ GeV/c^2 (for the η mode). The sideband regions are defined as $M(\pi^+\pi^-) \in (0.463, 0.483) \cup (0.513, 0.533)$ GeV/c^2, $M(\gamma\gamma) \in (0.08, 0.11) \cup (0.16, 0.19)$ GeV/c^2 (for the π^0 mode) and $M(\gamma\gamma) \in (0.44, 0.50) \cup (0.60, 0.66)$ GeV/c^2 (for the η mode). The signal yields at each energy, presented in Tables I and II, are obtained according to $N_{\rm sig} = N_{\rm A} - \sum N_{\rm B}/2 + \sum N_{\rm C}/4$, where N is the number of events and the subscript A denotes the signal region, and the subscripts B and C denote the sideband regions.

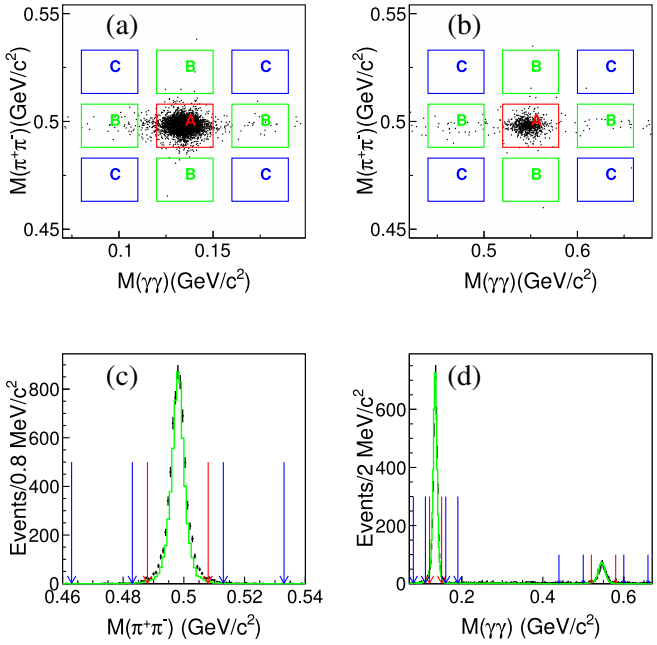

FIG. 1. The distributions of $M(\pi^+\pi^-)$ versus $M(\gamma\gamma)$ at $\sqrt{s} = 4.258$ GeV and the projections onto $M(\pi^+\pi^-)$ and $M(\gamma\gamma)$. (a) is the π^0 mode; (b) is the η mode; (c) is the $M(\pi^+\pi^-)$; (d) is the $M(\gamma\gamma)$. In plots (a) and (b), the boxes with mark "A" are the signal region and the boxes with marks "B" and "C" are sideband regions. In plots (c) and (d), the black error bars are the data, the green solid line is the PHSP MC simulation, the red arrows denote the signal regions, and the blue arrows denote the sideband regions.

The Born cross section is calculated from

$$\sigma_{\rm B} = \frac{N_{\rm sig}}{\mathcal{L} \cdot \mathcal{B} \cdot \epsilon \cdot (1+\delta^{\rm ISR}) \cdot \frac{1}{|1-\Pi(s)|^2}}, \qquad (1)$$

TABLE II. Same as Table I for $e^+e^- \to K_S^0 K^\pm \pi^\mp \eta$.

$\sqrt{s}$ (GeV)	$\mathcal{L}$ (pb^{-1})	$N_{\rm sig}$	ϵ (%)	$(1+\delta^{\rm ISR})$	$\frac{1}{\lvert 1-\Pi(s)\rvert^2}$	$\sigma_{\rm B}$ (pb)
3.896	52.61	76 ± 9	18.22	1.02	1.05	$27.23 \pm 3.22 \pm 1.26$
4.008	481.96	516 ± 24	18.19	1.04	1.04	$19.88 \pm 0.92 \pm 0.94$
4.085	52.63	42 ± 7	18.07	1.05	1.05	$14.71 \pm 2.45 \pm 0.70$
4.189	43.09	43 ± 7	17.92	1.09	1.06	$17.75 \pm 2.89 \pm 0.84$
4.208	54.55	43 ± 7	17.76	1.08	1.06	$14.20 \pm 2.31 \pm 0.61$
4.217	54.13	31 ± 6	18.06	1.09	1.06	$10.05 \pm 1.95 \pm 0.41$
4.226	1091.74	942 ± 31	17.85	1.08	1.06	$15.61 \pm 0.51 \pm 0.64$
4.242	55.59	45 ± 7	17.86	1.08	1.06	$14.63 \pm 2.28 \pm 0.60$
4.258	825.67	655 ± 26	17.75	1.08	1.05	$14.35 \pm 0.57 \pm 0.66$
4.308	44.90	32 ± 6	17.59	1.12	1.05	$12.67 \pm 2.38 \pm 0.55$
4.358	539.84	349 ± 19	17.79	1.12	1.05	$11.38 \pm 0.62 \pm 0.51$
4.387	55.18	40 ± 6	17.44	1.11	1.05	$13.05 \pm 1.96 \pm 0.62$
4.416	1073.56	638 ± 26	17.56	1.11	1.05	$10.62 \pm 0.43 \pm 0.49$
4.467	109.94	66 ± 8	17.23	1.14	1.06	$10.62 \pm 1.29 \pm 0.52$
4.527	109.98	45 ± 7	17.20	1.14	1.06	$7.27 \pm 1.31 \pm 0.37$
4.575	47.67	27 ± 5	17.29	1.15	1.06	$9.23 \pm 1.84 \pm 0.49$
4.600	566.93	288 ± 18	17.20	1.18	1.06	$8.67 \pm 0.54 \pm 0.43$

where $\mathcal{L}$ is the integrated luminosity, ϵ is the detection efficiency, $\mathcal{B}$ is the product of the BF of $K_S^0 \to \pi^+\pi^-$ and that of $\pi^0/\eta \to \gamma\gamma$ [57], $\frac{1}{\lvert 1-\Pi(s)\rvert^2}$ is the vacuum polarization correction factor [69], and $(1+\delta^{\rm ISR})$ is the ISR correction factor [70] which is determined by the MC simulation programmer KKMC. The ISR factors are set to 1.0 to get the initial cross section line shape as input to KKMC. From KKMC, the updated ISR factors are obtained, then the cross section line shape is updated too. We repeat this process until both ISR factors and cross section converge.

The invariant mass distributions of some two or three final state particles at $\sqrt{s} = 4.258$ GeV are shown in Figs. 2 and 3 as examples. There are some intermediate states observed in this four-body decay. To estimate the detection efficiency, a data-driven method is implemented to produce an exclusive MC sample that more closely resembles the data. We generate a mixing MC sample includes intermediate resonances, such as $\rho(770)$ and $K^*(892)$, with couplings tuned to match those appear in the data sample and is weighted according to the momentum distributions observed in the data sample. We choose each mixing channel by the order of the intermediate state significance. Then we set the mixing fractions by a rough fit to the two or three body invariant mass distributions and a further tuning. The mixing fractions are identical for all energy points. All mixing channels are generated using phase space (PHSP) generator. As illustrated in Figs. 2 and 3, the reweighted MC sample gives a much better description of the data than a PHSP MC sample. We verify that the remaining invariant mass, momentum, and angular distributions show equally good agreement between the reweighted MC and data. The observed cross sections are presented in Tables I and II, and illustrated in Fig. 4.

B. Upper limits of $e^+e^- \to Y(4260) \to K_S^0 K^\pm \pi^\mp \pi^0$ and $e^+e^- \to Y(4260) \to K_S^0 K^\pm \pi^\mp \eta$

Since there is no obvious structure in the line shapes of the Born cross sections for $e^+e^- \to K_S^0 K^\pm \pi^\mp \pi^0$ and $e^+e^- \to K_S^0 K^\pm \pi^\mp \eta$, as shown in Fig. 4, the upper limits of $Y(4260) \to K_S^0\, K^\pm\, \pi^\mp\, \pi^0$ and $Y(4260) \to K_S^0\, K^\pm\, \pi^\mp\, \eta$ are determined by fitting the line shapes with the function $\sigma_{\rm B}(\sqrt{s}) = f(\sqrt{s}) + {\rm BW}(\sqrt{s})$. Here $f(\sqrt{s}) = \frac{p_0}{(\sqrt{s})^{p_1}}$ describes the continuum process $e^+e^- \to K_S^0 K^\pm \pi^\mp \pi^0/\eta$, the parameters p_0 is left free in the fit, while p_1 is fixed to the result from a fit that only uses $f(\sqrt{s})$ to fit the line shapes. ${\rm BW}(\sqrt{s})$ given in Eq. (2)

$$ {\rm BW}(\sqrt{s}) = \frac{12\pi\Gamma_{e^+e^-}\mathcal{B}\Gamma_{\rm tot}}{(s-{\rm M}^2)^2 + {\rm M}^2\Gamma_{\rm tot}^2} \tag{2} $$

is a Breit-Wigner function describing the resonance $Y(4260)$, where M, $\Gamma_{\rm tot}$, and $\Gamma_{e^+e^-}$ are the mass, full width, and electronic width of $Y(4260)$, respectively; $\mathcal{B}$ is the branching fraction of the decay $Y(4260) \to K_S^0\, K^\pm\, \pi^\mp\, \pi^0/\eta$.

The mass and the full width of Y(4260) are set to the world average values 4230 ± 8 MeV/c^2 and 55 ± 19 MeV/c^2 [57]. The product $\Gamma_{e^+e^-}\mathcal{B}$ increases from 0 to 0.5 eV in step length of 0.001 eV. For each value of it, a fitting estimator Q^2 defined by Eq. (3)

$$ Q^2 = \sum_i \frac{(\sigma_{{\rm B}_i} - h\cdot\sigma_{{\rm B}_i}^{\rm fit})^2}{\delta_i^2} + \frac{(h-1)^2}{\delta_c^2} \tag{3} $$

is obtained. Here $\sigma_{\rm B}$ and $\sigma_{\rm B}^{\rm fit}$ are the measured and fitted Born cross sections, δ_i is the energy dependent part of the total uncertainty, which includes the statistical uncertainty and the energy dependent part of systematic uncertainty,

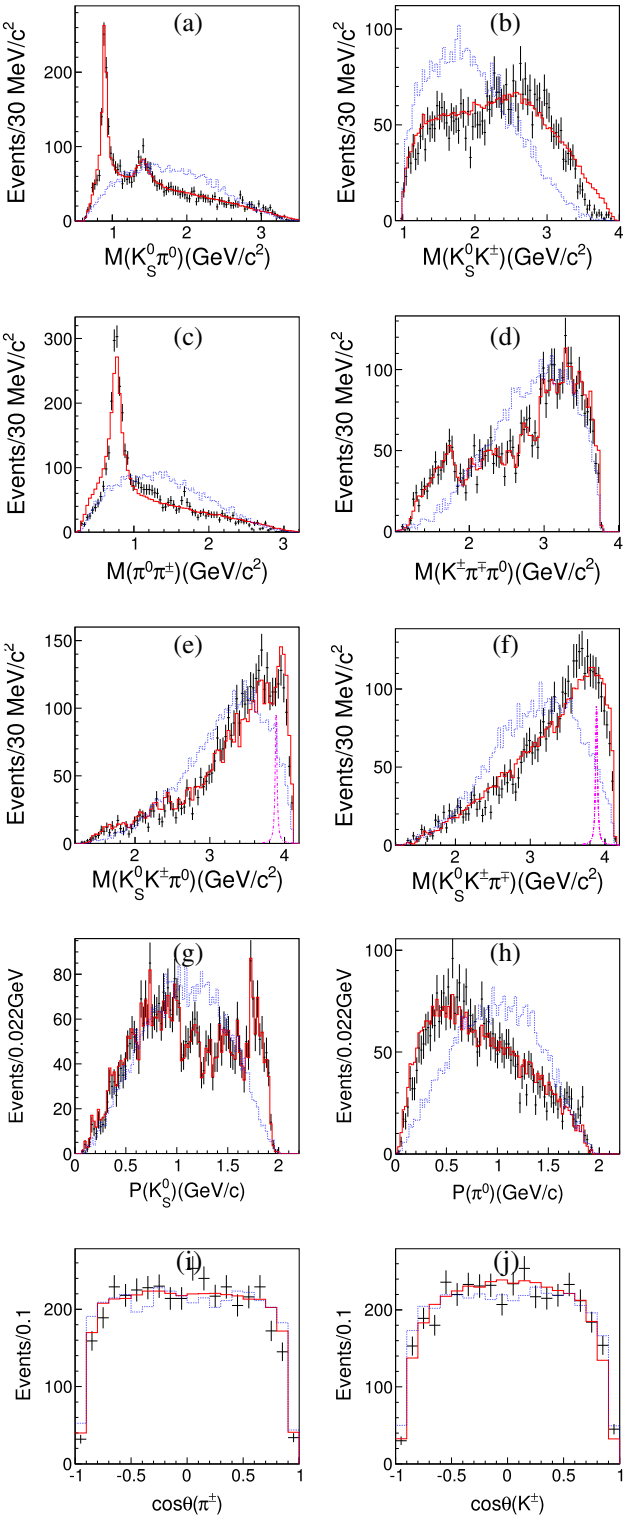

FIG. 2. Some invariant mass (M) distributions of two or three final state particles (a)–(f), momentum (P) distributions of final state particles (g),(h), polar angle (θ) distributions of final state particles (i),(j), in process $e^+e^- \to K^0_S K^\pm \pi^\mp \pi^0$ at 4.258 GeV as examples. The black dots with error bars are the data. The red solid lines are the mixing MC sample. The blue dashed lines are the PHSP MC sample. The pink dash-dotted lines in plot (i) and plot (j) are the MC shape of the $Z_c(3900)$ with an arbitrary scale.

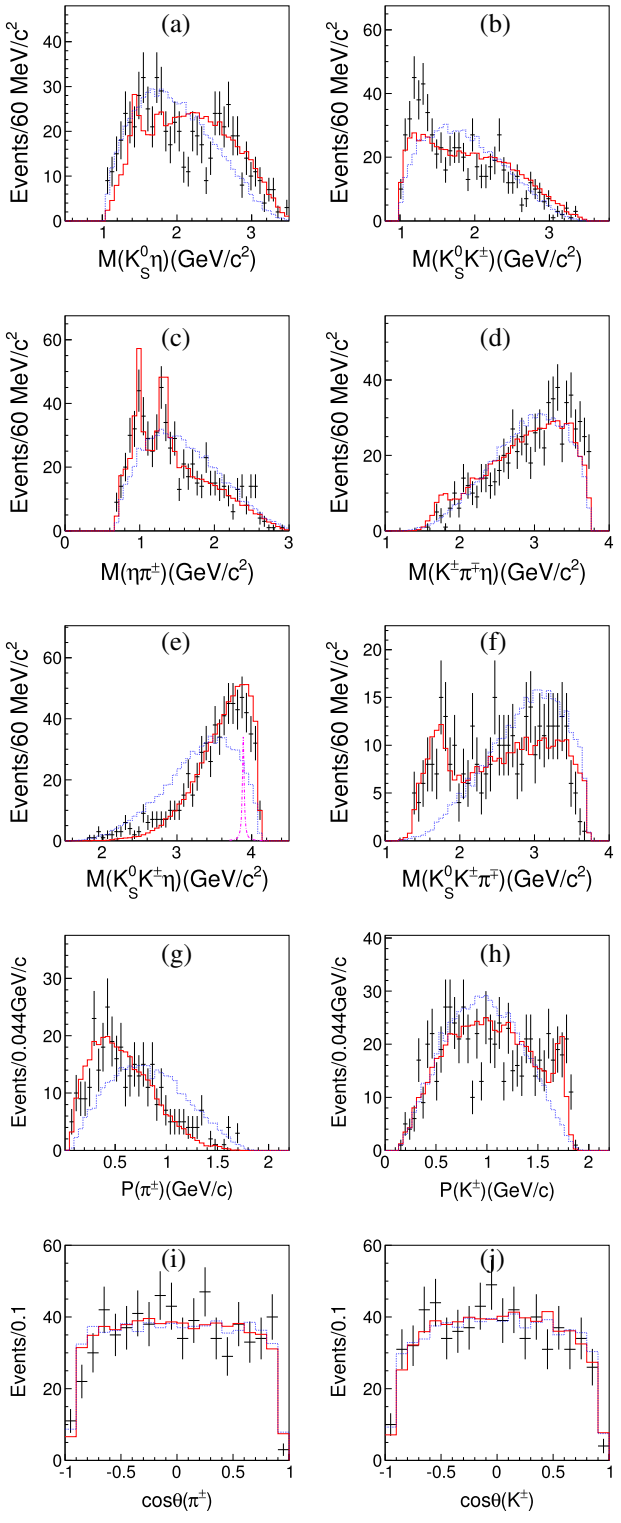

FIG. 3. Some invariant mass (M) distributions of two or three final state particles (a)–(f), momentum (P) distributions of final state particles (g),(h), polar angle (θ) distributions of final state particles (i),(j), in process $e^+e^- \to K^0_S K^\pm \pi^\mp \eta$ at 4.258 GeV as examples. The black dots with error bars are the data. The red solid lines are the mixing MC sample. The blue dashed lines are the PHSP MC sample. The pink dash-dotted lines in plot (i) are the MC shape of the $Z_c(3900)$ with an arbitrary scale.

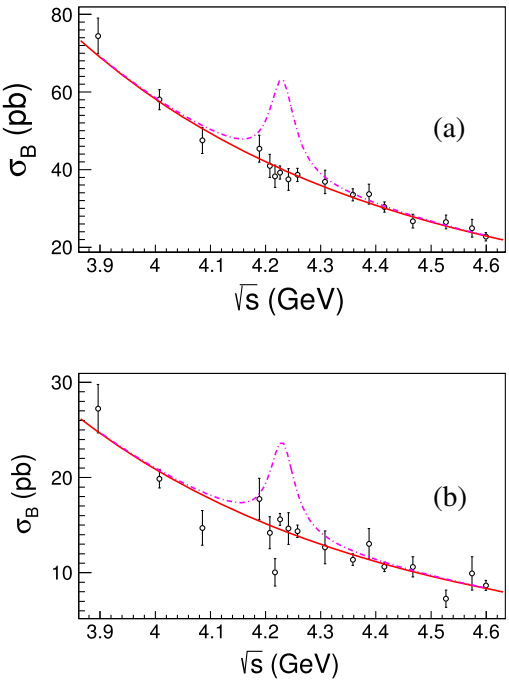

FIG. 4. Line shapes of Born cross sections for $e^+e^- \to K_S^0 K\pi\pi^0$ (a), and $e^+e^- \to K_S^0 K\pi\eta$ (b). The dots with error bars are the measured Born cross sections. The solid red lines are the fitted results with the function $f(\sqrt{s}) = \frac{p_0}{(\sqrt{s})^{p_1}}$ and parameters $p_0 = (6.14 \pm 1.54) \times 10^6$ (pb) $\cdot$ (GeV)^{p_1} and $p_1 = 6.68 \pm 0.17$ in the π^0 mode and $p_0 = (1.86 \pm 0.97) \times 10^5$ (pb) $\cdot$ (GeV)^{p_1} and $p_1 = 6.56 \pm 0.36$ in the η mode. The pink dash-dotted lines are the MC shape of the $Y(4260)$ with an arbitrary scale factor.

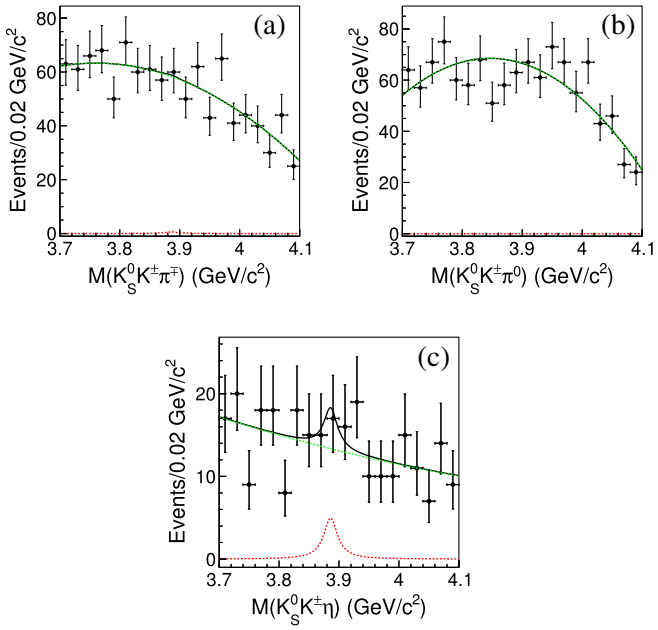

FIG. 5. The optimal fit for (a) $Z_c(3900)^0 \to K_S^0 K^\pm\pi^\mp$, (b) $Z_c(3900)^\pm \to K_S^0 K^\pm\pi^0$, and (c) $Z_c(3900)^\pm \to K_S^0 K^\pm\eta$ (at $\sqrt{s} = 4.258$ GeV as examples). The black error bars are the data, the black solid lines are the fit curve, the green dashed lines denote the background shape, and the red dashed lines denote the signal shape.

the δ_c is the energy independent part of the systematic uncertainty (the systematic uncertainties are described in detail in Sec. III D), h is a free parameter introduced to take into account the correlation of different energy points, and the subscript i indicates the index of each energy point [71]. The Q^2 is used to calculate the likelihood $L = e^{-0.5Q^2}$, whose normalized distribution is used to get the upper limits of $\Gamma_{e^+e^-}\mathcal{B}$ at the 90% confidence level (C.L.), which is determined to be 0.050 and 0.19 eV for the π^0 mode and the η mode, respectively.

C. Upper limits on $\sigma_B(e^+e^- \to \pi^{0,\mp} Z_c^{0,\pm}(3900), Z_c^{0,\pm}(3900) \to K_S^0 K^\pm \pi^{\mp,0}/\eta)$

Since there is no obvious $Z_c(3900)$ signal in the invariant mass distributions of $K_S^0 K^\pm\pi^{\mp,0}$ (π^0 mode) and $K_S^0 K^\pm\eta$ (η mode), as shown in Figs. 2 and 3, the upper limits at the 90% C.L. for the production cross section $\sigma_B(e^+e^- \to \pi Z_c(3900))$, with $Z_c(3900) \to K_S^0 K\pi/\eta$ are determined with an unbinned maximum likelihood fit to the invariant mass of $K_S^0 K\pi/\eta$. The fit is performed separately at five large integrated luminosity energy points 4.226, 4.258, 4.358, 4.416, and 4.600 GeV. The fit range is $(3.7, 4.1)$ GeV/c^2. The contribution of non-K_S^0 or non-π^0/η backgrounds is negligible. In the fit, the $Z_c(3900)$ signal is described by the MC simulated shape, and the mass and width of the $Z_c(3900)$ are set to theirs world average value 3886.6 ± 2.4 MeV/c^2 and 28.2 ± 2.6 MeV/c^2 [57], respectively. The background is described by a second order polynomial function. Fig. 5 shows the fit results at $\sqrt{s} = 4.258$ GeV as examples.

The normalized likelihood distribution of the Born cross section $L(\sigma_B)$ is determined by changing the number of signal events from 0 to 150 with a step size of 1. The upper limit (UL) at the 90% C.L. is calculated by solving the equation

$$0.1 = \int_{\rm UL}^{\infty} L(\sigma_B) d\sigma_B. \quad (4)$$

The final upper limits are shown in Table III, where all of the systematic uncertainties have been considered, the details of which are explained in Sec. III D. The ratio

$$R = \frac{\sigma_B(e^+e^- \to \pi Z_c(3900) \to \pi K_S^0 K\pi/\eta)}{\sigma_B(e^+e^- \to \pi Z_c(3900) \to \pi\pi J/\psi)}$$

is also given in Table III, where the cross sections for $e^+e^- \to \pi^\mp Z_c(3900)^\pm \to \pi^+\pi^- J/\psi$ and $e^+e^- \to \pi^0 Z_c(3900)^0 \to \pi^0\pi^0 J/\psi$ are from Refs. [48] and [72], respectively.

TABLE III. Upper limits on $\sigma_{\rm B}(e^+e^- \to \pi Z_c(3900), Z_c(3900) \to K_S^0 K\pi/\eta)$, and its ratio (R) to $\sigma_{\rm B}(e^+e^- \to \pi Z_c(3900), Z_c(3900) \to \pi J/\psi)$ at the 90% C.L.

	$\sqrt{s}$ (GeV)	$\sigma_{\rm B}$ (pb)	R
$e^+e^- \to \pi^0 Z_c(3900)^0$,	4.226	<0.24	$<2.5 \times 10^{-2}$
$Z_c(3900)^0 \to K_S^0 K^\pm \pi^\mp$	4.258	<0.38	$<1.2 \times 10^{-1}$
	4.358	<0.51	$<2.6 \times 10^{-1}$
	4.416	<0.27	···
	4.600	<0.33	···
$e^+e^- \to \pi^\pm Z_c(3900)^\mp$,	4.226	<0.17	$<9.1 \times 10^{-3}$
$Z_c(3900)^\mp \to K_S^0 K^\mp \pi^0$	4.258	<0.28	$<5.6 \times 10^{-2}$
	4.358	<0.57	···
	4.416	<0.34	···
	4.600	<0.45	···
$e^+e^- \to \pi^\pm Z_c(3900)^\mp$,	4.226	<0.18	$<1.0 \times 10^{-2}$
$Z_c(3900)^\mp \to K_S^0 K^\mp \eta$	4.258	<0.56	$<1.4 \times 10^{-1}$
	4.358	<0.53	···
	4.416	<0.76	···
	4.600	<0.58	···

D. Systematic uncertainties

Various sources of systematic uncertainty are investigated in the $e^+e^- \to K_S^0 K^\pm \pi^\mp \pi^0/\eta$ cross section measurements. We assume that the systematic uncertainties associated with the physics model used in the MC simulation, the luminosity, tracking, PID, γ reconstruction efficiency, K_S^0 reconstruction efficiency, ISR correction factor, vacuum polarization factor and quoted BFs are energy independent, while the other systematic effects are energy dependent.

For the π^0 mode, a data-driven MC method is developed to obtain the efficiency. To estimate the uncertainty of this method, one thousand testing samples of $e^+e^- \to K_S^0 K^\pm \pi^\mp \pi^0$ are generated with eighteen different physics processes with random ratios, the ratio of each process is generated using uniform distribution between 0 to 1 and then normalized by the summation of these eighteen ratios. The difference between the estimated and the real efficiencies is fitted with a Gaussian function. The fit results give a mean of 0.4% which is neglected, and a width of 0.9% which is taken as the systematic uncertainty from the data-driven MC method. For the η mode, which has much lower statistics than the π^0 mode, alternative mixing ratios are used to generate a new MC sample and the efficiency difference between the two MC samples is adopted as the systematic uncertainty.

The uncertainty on the integrated luminosity is estimated to be 1.0% using Bhabha events [60].

Both the uncertainties of tracking and particle identification (PID) for charged tracks originating at the interaction point are determined to be 1.0% per track using $J/\psi \to K_S^0 K^\pm \pi^\mp$, $J/\psi \to p\bar{p}\pi^+\pi^-$, and $J/\psi \to \pi^+\pi^-\pi^0$ [73] as control samples.

The uncertainty due to photon reconstruction efficiency is 1.0% per photon, which is derived from studies of $J/\psi \to \rho^0\pi^0, \rho^0 \to \pi^+\pi^-, \pi^0 \to \gamma\gamma$ [74].

The uncertainty associated with the K_S^0 reconstruction is studied using $J/\psi \to K^*(892)^\pm K^\mp, K^*(892)^\pm \to K_S^0\pi^\pm$ and $J/\psi \to \phi K_S^0 K^\pm \pi^\mp$ control samples and is estimated to be 1.2% [75].

The ISR correction factor introduces a 1.0% uncertainty since the termination condition of the recursion method used to get the correction factor is 1.0% between the last two iterations.

The uncertainty due to the vacuum polarization factor is found to be negligible [69]. The uncertainties of the quoted BFs are also considered.

The energy dependent ones include the systematic uncertainties from the choosing about mass window and sideband regions of K_S^0, π^0, and η and the kinematic fit. The uncertainties associated with the K_S^0, π^0, and η invariant mass regions are determined by changing them from $(0.488, 0.508)$ to $(0.483, 0.513)$ GeV/c^2, $(0.12, 0.15)$ to $(0.115, 0.155)$ GeV/c^2 and $(0.52, 0.58)$ to $(0.51, 0.59)$ GeV/c^2 for the K_S^0, π^0 and η, respectively. The differences in the efficiencies are taken as the corresponding systematic uncertainties.

The uncertainties due to the side-band regions are determined by changing the side-band region to $M_\eta \in (0.44, 0.47) \cup (0.63, 0.66)$ GeV/c^2, $M_{\pi^0} \in (0.08, 0.095) \cup (0.175, 0.19)$ GeV/c^2 and $M_{K_S^0} \in (0.463, 0.473) \cup (0.523, 0.533)$ GeV/c^2. The differences are taken as the associated systematic uncertainties.

The uncertainty associated with the kinematic fit is determined by comparing the efficiencies with and without corrections to the track helix parameters [76].

Assuming all sources of systematic uncertainties are independent, the total uncertainties are the sums of the individual values in quadrature (Table IV).

The systematic uncertainties that affect the upper limits on $\sigma_{\rm B}(e^+e^- \to \pi Z_c(3900), Z_c(3900) \to K_S^0 K\pi/\eta)$ are considered in two categories: multiplicative and nonmultiplicative. The nonmultiplicative systematic uncertainties on the signal shape and the background shape are considered by changing the signal shape to a Breit-Wigner function and varying the fit range, the parameters of the $Z_c(3900)$, and the order of the polynomial functions in the fit. The maximum upper limits are adopted for all combinations of these variations. The intermediate states in the $Z_c(3900)$ decay are considered by generating signal MC samples with alternative processes $Z_c(3900) \to K^*(892)K$, $K^*(892) \to K(K_S^0)\pi$ (π^0 mode), and $Z_c(3900) \to a_0(980)\eta$, $a_0(980) \to K_S^0 K$ (η mode). The efficiency difference is considered as a multiplicative systematic uncertainty. All of the systematic uncertainties, which are listed in Table IV, excluding the side-band item and mixing MC item, are considered as the multiplicative systematic uncertainties.

TABLE IV. Summary of systematic uncertainties (in %). The systematic uncertainties listed in this table are related to the born cross section measurements of processes $e^+e^- \to K_S^0K^\pm\pi^\mp\pi^0/\eta$ and the upper limits extracted work of $e^+e^- \to Y(4260) \to K_S^0K^\pm\pi^\mp\pi^0/\eta$ and $e^+e^- \to \pi Z_c(3900) \to K_S^0K^\pm\pi^\mp\pi^0/\eta$.

	$\sqrt{s}$ (GeV)	3.896	4.008	4.085	4.189	4.208	4.217	4.226	4.242	4.258	4.308	4.358	4.387	4.416	4.467	4.527	4.575	4.600
Both mode	$\mathcal{L}$	1.0	1.0	1.0	1.0	1.0	1.0	1.0	1.0	1.0	1.0	1.0	1.0	1.0	1.0	1.0	1.0	1.0
	K_S^0 reconstruction	1.2	1.2	1.2	1.2	1.2	1.2	1.2	1.2	1.2	1.2	1.2	1.2	1.2	1.2	1.2	1.2	1.2
	Tracking	2.0	2.0	2.0	2.0	2.0	2.0	2.0	2.0	2.0	2.0	2.0	2.0	2.0	2.0	2.0	2.0	2.0
	PID	2.0	2.0	2.0	2.0	2.0	2.0	2.0	2.0	2.0	2.0	2.0	2.0	2.0	2.0	2.0	2.0	2.0
	γ reconstruction	2.0	2.0	2.0	2.0	2.0	2.0	2.0	2.0	2.0	2.0	2.0	2.0	2.0	2.0	2.0	2.0	2.0
	$\mathrm{BF}_{K_S^0\to\pi^+\pi^-}$	0.1	0.1	0.1	0.1	0.1	0.1	0.1	0.1	0.1	0.1	0.1	0.1	0.1	0.1	0.1	0.1	0.1
	$(1+\delta^{\mathrm{ISR}})$	1.0	1.0	1.0	1.0	1.0	1.0	1.0	1.0	1.0	1.0	1.0	1.0	1.0	1.0	1.0	1.0	1.0
π^0 mode	Mixing MC	0.9	0.9	0.9	0.9	0.9	0.9	0.9	0.9	0.9	0.9	0.9	0.9	0.9	0.9	0.9	0.9	0.9
	Kinematic fit	0.3	0.3	0.3	0.3	0.3	0.4	0.3	0.3	0.4	0.1	0.2	0.2	0.2	0.4	0.4	0.3	0.4
	π^0 mass interval	0.6	0.6	0.6	0.6	0.6	0.6	0.6	0.6	0.5	0.5	0.6	0.6	0.6	0.6	0.8	0.8	0.8
	K_S^0 mass interval	0.1	0.1	0.1	0.1	0.1	0.1	0.1	0.1	0.3	0.3	0.2	0.3	0.3	0.3	0.2	0.2	0.2
	Side band	0.2	0.2	0.2	0.2	0.1	0.1	0.1	0.1	0.1	0.1	0.1	0.1	0.1	0.1	0.1	0.1	0.1
	$\mathrm{BF}_{\pi^0\to\gamma\gamma}$	0.1	0.1	0.1	0.1	0.1	0.1	0.1	0.1	0.1	0.1	0.1	0.1	0.1	0.1	0.1	0.1	0.1
	Total	4.1	4.1	4.1	4.1	4.1	4.1	4.1	4.1	4.1	4.1	4.1	4.1	4.1	4.1	4.1	4.1	4.1
η mode	Mixing MC	0.2	1.4	1.1	1.0	1.2	0.3	0.1	0.4	1.6	0.5	1.4	1.2	0.3	1.6	1.5	0.6	0.9
	Kinematic fit	0.3	0.2	0.2	0.2	0.2	0.2	0.2	0.3	0.3	0.2	0.1	0.3	0.4	0.1	0.2	0.2	0.2
	η mass interval	1.6	1.6	1.6	1.6	0.6	0.6	0.6	0.6	0.9	0.9	1.0	0.4	0.4	0.4	1.7	1.7	1.7
	K_S^0 mass interval	1.7	1.7	1.7	1.7	0.7	0.7	0.7	0.7	1.4	1.4	1.1	2.1	2.1	2.1	2.3	2.3	2.3
	Side band	0.1	0.1	0.1	0.1	0.6	0.6	0.6	0.6	0.5	0.5	0.4	1.1	1.1	1.1	0.4	0.4	0.4
	$\mathrm{BF}_{\eta\to\gamma\gamma}$	0.5	0.5	0.5	0.5	0.5	0.5	0.5	0.5	0.5	0.5	0.5	0.5	0.5	0.5	0.5	0.5	0.5
	Total	4.6	4.8	4.7	4.7	4.3	4.1	4.1	4.1	4.6	4.4	4.5	4.8	4.7	4.9	5.1	4.9	5.0

The effects of multiplicative systematic uncertainties are taken into account by convolving the distribution of $L(\sigma_{\mathrm{B}})$ with a probability distribution function of sensitivity (S), which is assumed to be a Gaussian function with central value $\hat{S}$ and standard deviation δ_S [77]:

$$L'(\sigma_{\mathrm{B}}) = \int_0^1 L\left(\frac{S}{\hat{S}}\sigma_{\mathrm{B}}\right)\cdot e^{-\frac{(S-\hat{S})^2}{2\delta_s^2}}dS. \tag{5}$$

Here S is the sensitivity that refers to the denominator of Eq. (1) and δ_s is the total multiplicative systematic uncertainty. $L'(\sigma_{\mathrm{B}})$ is the likelihood distribution of the Born cross section after the multiplicative systematic uncertainties are incorporated.

IV. SUMMARY

The Born cross sections for $e^+e^- \to K_S^0K^\pm\pi^\mp\pi^0$ and $K_S^0K^\pm\pi^\mp\eta$ are measured with data samples collected at center-of-mass energies from 3.90 to 4.60 GeV. Since no clear structure is observed, the upper limits of the product $\Gamma_{e^+e^-}\mathcal{B}$ $(Y(4260) \to K_S^0K^\pm\pi^\mp\pi^0)$ at 90% C.L. are estimated to be less than 0.05 eV and that of $\Gamma_{e^+e^-}\mathcal{B}(Y(4260) \to K_S^0K^\pm\pi^\mp\eta)$ is estimated to be smaller than 0.19 eV. Reference [9] reported four solutions of the product $\Gamma_{e^+e^-}\mathcal{B}(Y(4260) \to \pi^+\pi^-J/\psi)$, in which the maximum is 13.3 ± 1.4 eV and the minimum is 1.5 ± 0.3 eV. Comparing them with our results, the branching fraction of the $Y(4260)$ decaying into $K_S^0K^\pm\pi^\mp\pi^0$ and $K_S^0K^\pm\pi^\mp\eta$ is much smaller, which indicates a much smaller coupling of the $Y(4260)$ to the light hadrons $K_S^0K^\pm\pi^\mp\pi^0$ and $K_S^0K^\pm\pi^\mp\eta$. We also search for $e^+e^- \to \pi Z_c(3900)$, $Z_c(3900) \to K_S^0K\pi/\eta$ and no obvious $Z_c(3900)$ signal is observed in the charged or neutral mode. The 90% C.L. upper limits on the cross sections are given at $\sqrt{s} = 4.226$, 4.258, 4.358, 4.416, and 4.600 GeV. The absence of a signal suggests that the cross sections for light hadron decay modes are small and that the annihilation of $c\bar{c}$ in the $Y(4260)$ and $Z_c(3900)$ is suppressed. Additional exploration of light hadron decay modes is needed to confirm the hypotheses.

ACKNOWLEDGMENTS

The BESIII Collaboration thanks the staff of BEPCII and the IHEP computing center for their strong support. This work is supported in part by National Key Basic Research Program of China under Contract No. 2015CB856700; National Natural Science Foundation of China (NSFC) under Contracts No. 11335008, No. 11425524, No. 11625523, No. 11635010, No. 11735014; the Chinese Academy of Sciences (CAS) Large-Scale Scientific Facility Program; the CAS Center for Excellence in Particle Physics (CCEPP); Joint Large-Scale Scientific Facility Funds of the NSFC and CAS under Contracts No. U1532257, No. U1532258, No. U1732263; CAS Key Research Program of Frontier

Sciences under Contracts No. QYZDJ-SSW-SLH003, No. QYZDJ-SSW-SLH040; 100 Talents Program of CAS; INPAC and Shanghai Key Laboratory for Particle Physics and Cosmology; German Research Foundation DFG under Contracts No. Collaborative Research Center CRC 1044, No. FOR 2359; Istituto Nazionale di Fisica Nucleare, Italy; Koninklijke Nederlandse Akademie van Wetenschappen (KNAW) under Contract No. 530-4CDP03; Ministry of Development of Turkey under Contract No. DPT2006K-120470; National Science and Technology fund; The Swedish Research Council; U.S. Department of Energy under Contracts No. DE-FG02-05ER41374, No. DE-SC-0010118, No. DE-SC-0010504, No. DE-SC-0012069; University of Groningen (RuG) and the Helmholtzzentrum fuer Schwerionenforschung GmbH (GSI), Darmstadt. This paper is also supported by Joint Large-Scale Scientific Facility Funds of the NSFC and CAS, Grant No. U1632104.

[1] H. X. Chen, W. Chen, X. Liu, and S. L. Zhu, Phys. Rep. **639**, 1 (2016).
[2] A. Ali, J. S. Lange, and S. Stone, Prog. Part. Nucl. Phys. **97**, 123 (2017).
[3] B. Aubert *et al.* (*BABAR* Collaboration), Phys. Rev. Lett. **95**, 142001 (2005).
[4] Q. He *et al.* (CLEO Collaboration), Phys. Rev. D **74**, 091104 (2006).
[5] C. Z. Yuan *et al.* (Belle Collaboration), Phys. Rev. Lett. **99**, 182004 (2007).
[6] J. P. Lees *et al.* (*BABAR* Collaboration), Phys. Rev. D **86**, 051102 (2012).
[7] T. E. Coan *et al.* (CLEO Collaboration), Phys. Rev. Lett. **96**, 162003 (2006).
[8] M. Ablikim *et al.* (BESIII Collaboration), Phys. Rev. Lett. **114**, 092003 (2015).
[9] M. Ablikim *et al.* (BESIII Collaboration), Phys. Rev. Lett. **118**, 092001 (2017).
[10] M. Ablikim *et al.* (BESIII Collaboration), Phys. Rev. D **96**, 032004 (2017).
[11] M. Ablikim *et al.* (BESIII Collaboration), Phys. Rev. Lett. **118**, 092002 (2017).
[12] M. Ablikim *et al.* (BESIII Collaboration), arXiv:1808.02847.
[13] B. Aubert *et al.* (*BABAR* Collaboration), Phys. Rev. D **76**, 111105 (2007).
[14] G. Pakhlova *et al.* (Belle Collaboration), Phys. Rev. Lett. **98**, 092001 (2007).
[15] G. Pakhlova *et al.* (Belle Collaboration), Phys. Rev. Lett. **100**, 062001 (2008).
[16] G. Pakhlova *et al.* (Belle Collaboration), Phys. Rev. D **80**, 091101 (2009).
[17] D. Cronin-Hennessy *et al.* (CLEO Collaboration), Phys. Rev. D **80**, 072001 (2009).
[18] B. Aubert *et al.* (*BABAR* Collaboration), Phys. Rev. D **79**, 092001 (2009).
[19] P. del Amo Sanchez *et al.* (*BABAR* Collaboration), Phys. Rev. D **82**, 052004 (2010).
[20] Z. Q. Liu, X. S. Qin, and C. Z. Yuan, Phys. Rev. D **78**, 014032 (2008).
[21] X. L. Wang *et al.* (Belle Collaboration), Phys. Rev. D **87**, 051101 (2013).
[22] B. Aubert *et al.* (*BABAR* Collaboration), Phys. Rev. D **74**, 091103 (2006).
[23] B. Aubert *et al.* (*BABAR* Collaboration), Phys. Rev. D **77**, 092002 (2008).
[24] B. Aubert *et al.* (*BABAR* Collaboration), Phys. Rev. D **73**, 012005 (2006).
[25] F. J. Llanes-Estrada, Phys. Rev. D **72**, 031503 (2005).
[26] M. Shah, A. Parmar, and P. C. Vinodkumar, Phys. Rev. D **86**, 034015 (2012).
[27] B. Q. Li and K. T. Chao, Phys. Rev. D **79**, 094004 (2009).
[28] A. Zhang, Phys. Lett. B **647**, 140 (2007).
[29] S. L. Zhu, Phys. Lett. B **625**, 212 (2005).
[30] E. Kou and O. Pene, Phys. Lett. B **631**, 164 (2005).
[31] L. Maiani, F. Piccinini, A. D. Polosa, and V. Riquer, Phys. Rev. D **72**, 031502 (2005).
[32] N. V. Drenska, R. Faccini, and A. D. Polosa, Phys. Rev. D **79**, 077502 (2009).
[33] D. Ebert, R. N. Faustov, and V. O. Galkin, Phys. Lett. B **634**, 214 (2006).
[34] D. Ebert, R. N. Faustov, and V. O. Galkin, Eur. Phys. J. C **58**, 399 (2008).
[35] C. Z. Yuan, P. Wang, and X. H. Mo, Phys. Lett. B **634**, 399 (2006).
[36] G. J. Ding, Phys. Rev. D **79**, 014001 (2009).
[37] F. Close and C. Downum, Phys. Rev. Lett. **102**, 242003 (2009).
[38] F. Close, C. Downum, and C. E. Thomas, Phys. Rev. D **81**, 074033 (2010).
[39] M. Cleven, Q. Wang, F. K. Guo, C. Hanhart, Ulf-G. Meissner, and Q. Zhao, Phys. Rev. D **90**, 074039 (2014).
[40] T. W. Chiu and T. H. Hsieh (TWQCD Collaboration), Phys. Rev. D **73**, 094510 (2006).
[41] E. van Beveren and G. Rupp, Phys. Rev. D **79**, 111501 (2009).
[42] E. van Beveren, G. Rupp, and J. Segovia, Phys. Rev. Lett. **105**, 102001 (2010).
[43] D. Y. Chen, J. He, and X. Liu, Phys. Rev. D **83**, 054021 (2011).
[44] M. Ablikim *et al.* (BESIII Collaboration), Phys. Rev. Lett. **110**, 252001 (2013).
[45] M. Ablikim *et al.* (BESIII Collaboration), Phys. Rev. Lett. **112**, 022001 (2014).
[46] M. Ablikim *et al.* (BESIII Collaboration), Phys. Rev. D **92**, 092006 (2015).
[47] M. Ablikim *et al.* (BESIII Collaboration), Phys. Rev. Lett. **115**, 222002 (2015).

[48] M. Ablikim *et al.* (BESIII Collaboration), Phys. Rev. Lett. **119**, 072001 (2017).
[49] F. K. Guo, C. Hidalgo-Duque, J. Nieves, and M. Pavón Valderrama, Phys. Rev. D **88**, 054007 (2013).
[50] L. Maiani, V. Riquer, R. Faccini, F. Piccinini, A. Pilloni, and A. D. Polosa, Phys. Rev. D **87**, 111102 (2013).
[51] E. S. Swanson, Phys. Rev. D **91**, 034009 (2015).
[52] Q. Wang, C. Hanhart, and Q. Zhao, Phys. Rev. Lett. **111**, 132003 (2013).
[53] D. Y. Chen, X. Liu, and T. Matsuki, Phys. Rev. Lett. **110**, 232001 (2013).
[54] M. Ablikim *et al.* (BESIII Collaboration), Phys. Rev. D **92**, 032009 (2015).
[55] M. Ablikim *et al.* (BESIII Collaboration), Phys. Lett. B **771**, 45 (2017).
[56] M. Ablikim *et al.* (BESIII Collaboration), Phys. Lett. B **774**, 78 (2017).
[57] M. Tanabashi *et al.* (Particle Data Group), Phys. Rev. D **98**, 030001 (2018).
[58] M. Ablikim *et al.* (BESIII Collaboration), Nucl. Instrum. Methods Phys. Res., Sect. A **614**, 345 (2010).
[59] C. Zhang *et al.*, Sci. China Phys. Mech. Astron. **53**, 2084 (2010).
[60] M. Ablikim *et al.* (BESIII Collaboration), Chin. Phys. C **39**, 093001 (2015).
[61] M. Ablikim *et al.* (BESIII Collaboration), Chin. Phys. C **40**, 063001 (2016).
[62] S. Agostinelli *et al.* (GEANT4 Collaboration), Nucl. Instrum. Methods Phys. Res., Sect. A **506**, 250 (2003).
[63] Z. Y. Deng *et al.*, Chin. Phys. C **30**, 371 (2006).
[64] D. J. Lange, Nucl. Instrum. Methods Phys. Res., Sect. A **462**, 152 (2001).
[65] R. G. Ping, Chin. Phys. C **32**, 599 (2008).
[66] S. Jadach, B. F. L. Ward, and Z. Was, Phys. Rev. D **63**, 113009 (2001).
[67] G. Balossini, C. M. C. Calame, G. Montagna, O. Nicrosini, and F. Piccinini, Nucl. Phys. **B758**, 227 (2006).
[68] M. Xu *et al.*, Chin. Phys. C **33**, 428 (2009).
[69] S. Actis *et al.*, Eur. Phys. J. C **66**, 585 (2010).
[70] E. A. Kuraev and V. S. Fadin, Sov. J. Nucl. Phys. **41**, 466 (1985).
[71] X. H. Mo, HEP & NP **31**, 745 (2007).
[72] M. Ablikim *et al.* (BESIII Collaboration), Phys. Rev. Lett. **115**, 112003 (2015).
[73] M. Ablikim *et al.* (BESIII Collaboration), Phys. Rev. D **83**, 112005 (2011).
[74] M. Ablikim *et al.* (BESIII Collaboration), Phys. Rev. D **81**, 052005 (2010).
[75] M. Ablikim *et al.* (BESIII Collaboration), Phys. Rev. D **92**, 112008 (2015).
[76] M. Ablikim *et al.* (BESIII Collaboration), Phys. Rev. D **87**, 012002 (2013).
[77] K. Stenson, arXiv:physics/0605236.